3.2 Doping of Cr_2O_3 Thin Films

The resistivity of the Cr_2O_3 thin films showed strong dependence on thin film orientation. To improve and taylor the conductivity, it is tried to incorporate acceptors into the *p*-type material. The elements chosen for this are Cu and Zn, because doping has already been accomplished on *c*-plane sapphire with magnesium via MgO [1]. Furthermore, it is tried to reduce the sheet resistance of the contacts of the thin films.

3.2.1 Experiment

To fabricate doped thin films, three different PLD targets were applied. Each target was eliptically segmented (cf. 2.1.1), with the outer region consisting of pure Cr_2O_3. The inner region (ellipse) was also Cr_2O_3 but with a fraction of dopant, namely:

1. 0.01 wt.% CuO, called "CuO-doped",
2. 0.01 wt.% ZnO, called "ZnO-doped (low)" and
3. 1 wt.% ZnO, called "ZnO-doped (high)".

For each target, several processes were done with the laser spot position varying on the target. For each process, deposition was done on all of the 4 aforementioned substrate orientations to check whether the conductivity of the prismatic orientations could be improved. The composition of the ablated material can be calculated via Equ. 2.1, but this does not account for the finite area illuminated by the laser pulse. A simple model for including this effect can be achieved by simulating N several randomly distributed points r_i in the range Δr around a radial laser position r_{PLD}. Then, the composition x_D can be calculated as the mean of the N calculated compositions for each r_i. The resulting dependence of x_D on r_{PLD} is visualized in Fig. 3.11a, where a higher value of Δr results in more smeared out graphs. A target with inner concentration of 0.01 wt.% dopant was assumed (Cu-doped target or Zn-doped (low) target). The Monto Carlo simulations can further be approximated by a linear fit, which was done for $\Delta r = 2\,\mathrm{mm}$ (blue dotted line in Fig. 3.11a). Henceforth, the different samples fabricated with different radial laser spot positions r_{PLD} are characterized by the expected composition x_D calculated from this linear fit. The reason for this is that according to Equ. 2.1, when applying r_{PLD} smaller than the length of the semi-minor axis of the inner ellipse, no variation in composition would be observed, even though the real finite laser spot size results in a different result. Note further that due to the small concentration of dopant, it is not possible to resolve those fractions via element sensitive measurements. Dr. Daniel Splith kindly performed Energy-dispersive X-Ray Spectroscopy (EDX) measurements that resulted in no signal for either Cu or Zn that was above the noise level.

To improve the contacts for resistivity measurements, samples were produced using the ZnO-doped (low) target and a fixed $r_{\mathrm{PLD}} = 3\,\mathrm{mm}$. Only *c*- and *r*-plane sapphire substrates were used and the deposition temperature was varied between 560 °C and 680 °C. For each growth temperature, subsequent contacting was done with Ti-Al-Au for a *c*-plane and an *r*-plane sample, as well as Ti-Au for a *c*-plane and an *r*-plane sample. Furthermore, the *c*-plane samples contacted with Ti-Al-Au were compared before and after annealing at 210 °C in nitrogen atomosphere.

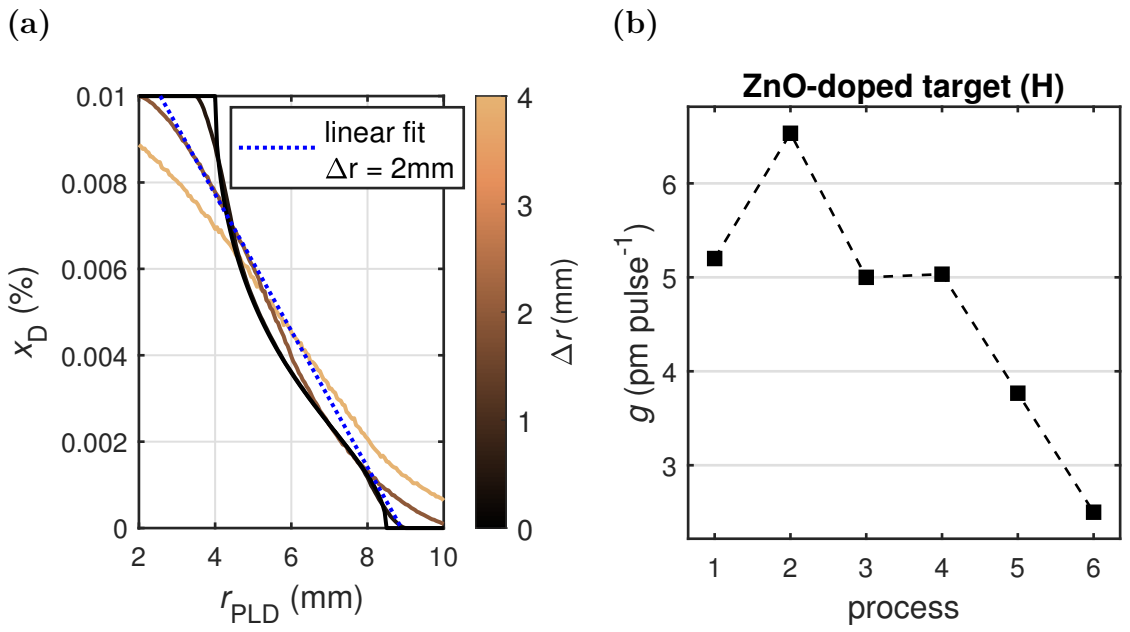

Figure 3.11: **(a)** Predictions for the plasma plume composition x_D using Monte Carlo simulations with $N = 10\,000$ and different values for Δr. The blue dotted line is a fit for the Graph calculated with $r = 2\,\text{mm}$. **(b)** Growth rate depending on the process order for the samples fabricated from the ZnO-doped (high) target. The laser entrance window was cleaned after each process.

2ϑ-ω-scans were performed for every sample, but ω-scans for c- and r-plane samples only. The thickness was determined using spectroscopic ellipsometry. Resistivity measurements at room temperature were done using the Pauw method, which was also applied when conducting temperature dependent resistivity measurements on one c-plane sample of each target. Note that the effect of infrequent cleaning of the laser entrance window that was described in 3.1 was discovered during the execution of those experiments, which is why the samples produced from the ZnO-doped (high) target were the only ones for which this effect could be prevented. Furthermore, 40 000 pulses were applied for the samples fabricated from the CuO-doped and ZnO-doped (low) target, as well as one sample from the batch made with the ZnO-doped (high) target. All other samples from this batch were deposited with 30 000 pulses.

3.2.2 Results

Laser Position Variation for Different Targets

The growth rates of the samples produced from the CuO-doped and ZnO-doped (low) target are depicted in Fig. 3.12. The growth rates vary between 3 and 6 pm pulse^{-1} and depend strongly on the number of deposition processes that were conducted before. After cleaning the laser entrance window, and thus reducing laser energy absorption, the growth rate can be increased. This is similar to the results obtained in 3.1.

However, the growth rates depending on the fabrication order for the ZnO-doped (high) samples are depicted in Fig. 3.11b. Note that the growth rate varies from approx. 2.5 to 6.5 pm pulse^{-1}, even though the laser entrance window was cleaned after each

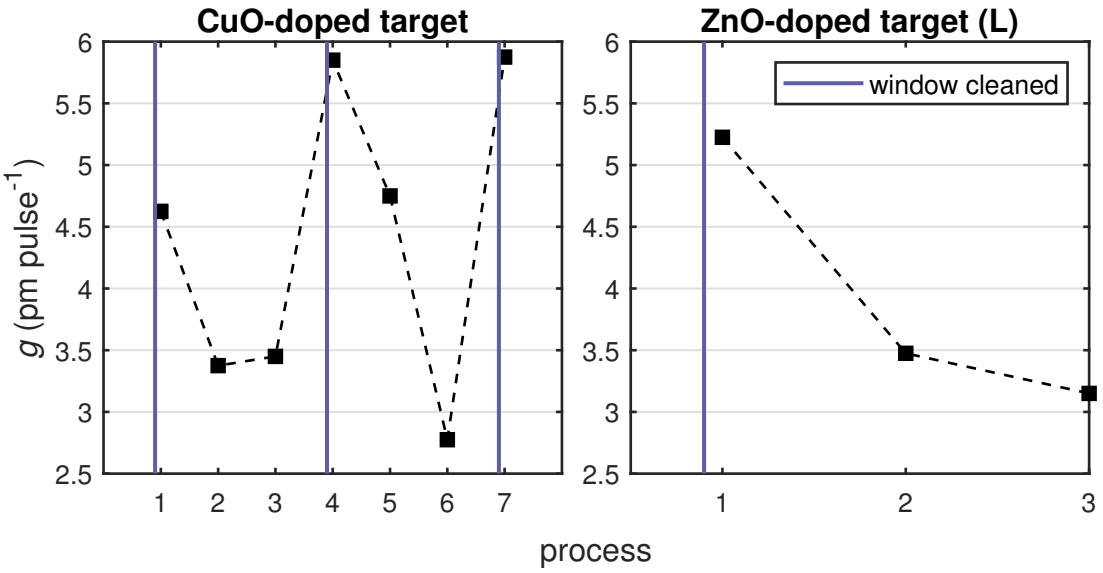

Figure 3.12: Growth rate depending on the process order for the samples fabricated from the CuO-doped and ZnO-doped (low) target. It is indicated when the laser entrance windows was cleaned.

process. So this variation in growth rate must be traced back to another effect. Only the first sample was fabricated with 40 000 pulses, which explains the increment of growth rate between the first and second process: Due to the higher number of pulses, the laser entrance window gets more coated and thus the last 10 000 pulses reduce the average growth rate. Furthermore, the second process was done with $r_{\mathrm{PLD}} = 6\,\mathrm{mm}$, which is rather outside compared to the 1st, 3rd and 4th process with 3 mm, 4 mm and 2 mm, respectively. This results in a larger total ablated area and in less target degradation. Therefore, the hypothesis is that target degradation during deposition has an influence on the growth rate. This is supported by the observation of incremental reduction of growth rate for processes 1, 5 and 6. Note that all these samples were fabricated with $r_{\mathrm{PLD}} = 3\,\mathrm{mm}$ and otherwise the same deposition parameters. The only variation is that tracks are carved into the target by the laser (Fig. 3.13c). This is probably the reason for a crucial change in plasma dynamics and therefore a reduction of the growth rate from approx. 5 to 2.5 pm pulse^{-1}.

For the samples with high conductivity, namely c-plane and r-plane, ω-scans were performed on the (00.6) and (02.4) reflection, respectively. The extracted ω-FWHMs are depicted in Fig. 3.14 depending on the growth rate for the respective process. A general trend is that the crystallinty increases for lower growth rates. It is not relevent, whether this reduction in growth rate ist due to less fluence on the laser target due to infrequent window cleaning (CuO-doped and ZnO-doped (low) target) or due to target degradation (ZnO-doped (high) target). The better FWHM is achieved for c-plane samples. Note that for the deposition of Cr_2O_3 on r-plane sapphire from the ZnO-doped (high) target, no thin film peaks in 2ϑ-ω-scans (see below) were observed. Those X-ray-amorphous films are presumably a result of the drastically altered plasma dynamics due to target degradation.

In Fig. 3.15a, the measured resistivity at room temperature depending on the predicted dopant concentration is depicted. From the unsystematic variation in resistivity

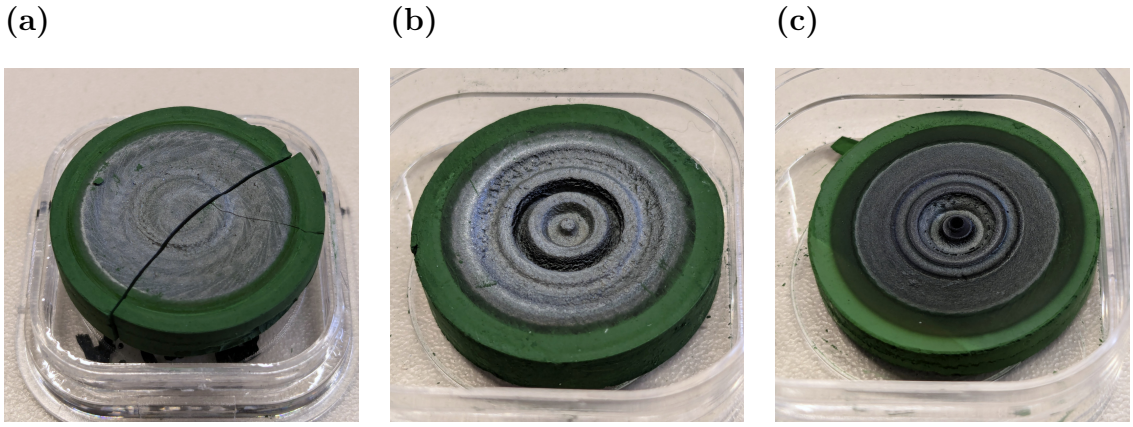

Figure 3.13: Photograph of the **(a)** CuO-doped, **(b)** ZnO-doped (low) and **(c)** ZnO-doped (high) target. The CuO-doped target broke during the last process where it was used. The silverish tint is presuambly due to formation of metallic chromium oxide on the target surface.

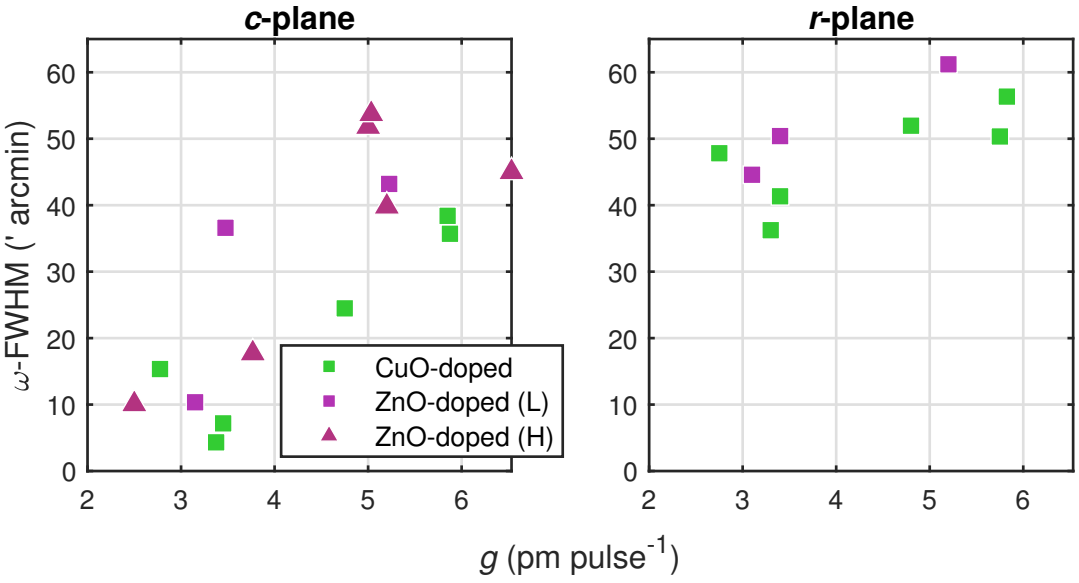

Figure 3.14: ω-FWHM for *c*- and *r*-plane samples that were fabricated from the three radially segmented targets.

Table 3.2: Activation energies E_A extracted from the linear regimes in the temperature dependent resistivity measurements (Fig. 3.16).

target	E_A (meV)	
	$< 100\,\mathrm{K}$	$> 100\,\mathrm{K}$
CuO-doped	53	83
ZnO-doped (low)	35	61
ZnO-doped (high)	31	50
pure Cr_2O_3	35	54

(2 to $500\,\Omega\,\mathrm{cm}$), it can be concluded that the attempt of doping the Cr_2O_3 thin films resulted in no improvement of conductivity. Using the two targets with different concentration of ZnO in the inner ellipse, no change was observed when adjusting x_D between 0.001 % and 1 %. Note the aforementioned samples that were all fabricated with $r_{\mathrm{PLD}} = 3\,\mathrm{mm}$ on the ZnO-doped (high) target, corresponding to the triangles in Fig. 3.15a at approx. $x_D = 1\,\%$: here, the same process parameters yield samples differing in resistivity by 2 orders of magnitude. Because those samples showed different growth rates due to target degradation, it is plausible that this also influences the conductivity.

The growth rate influences the crystal quality (cf. Fig. 3.14) and therefore, in Fig. 3.15b, the resistivity depending on the ω-FWHM is depicted. It becomes clear that a higher mosaicity results in higher conductivity. Since more dislocations correspond to more crystal defects (cf. 1.3.2), this result is in accordance to the predicted influence of crystal defects on the electrical properties of Cr_2O_3 thin films (cf. 1.2.1). It has to be noted that this effect is less pronounced for *r*-plane samples compared to *c*-plane samples. Furthermore, this does not explain why *m*- and *a*-plane Cr_2O_3 exhibit such higher resistivity, because their ω-FWHM is comparable to the basal and pyramidal orientations (cf. Tab. 3.1).

For each target, one *c*-plane sample with presumably highest doping concentration (smallest r_{PLD}) was chosen to perform temperature dependent resistivity measurements in the range of 40 to 390 K (Fig. 3.16). For all samples, an ARRHENIUS-like behavior is observed with two linear regimes above and below 100 K, respectively. By applying Equ. 3.3, two activation energies can be extracted that are listed in Tab. 3.2.[7] Note that the (arbitrary) choice, which samples were measured for each target, determined the absolute difference in resistivity: There are in fact samples fabricated from the CuO-doped target that have lower resistivity than samples fabricated from the ZnO-doped targets (cf. Fig. 3.15).

Even though the doping resulted in no improvement of the electrical properties of the thin films, the several samples fabricated at different growth conditions[8] may serve as an insight into the o.o.p. strain that was already observed in 3.1. To check whether the hypothesis of increasing strain with increasing growth rate is also true for orientations other than *m*-plane, the o.o.p. strain dependent on the growth rate is depicted in

[7] **Soll ich dazu noch mehr sagen? Ich weiß nicht, ob man sehr viel aus diesen Zahlen lernen kann.**

[8] Even though these differences were achieved accidentally: by infrequent laser entrance window cleaning and repeated ablation on targets with the same laser spot position r_{PLD}.

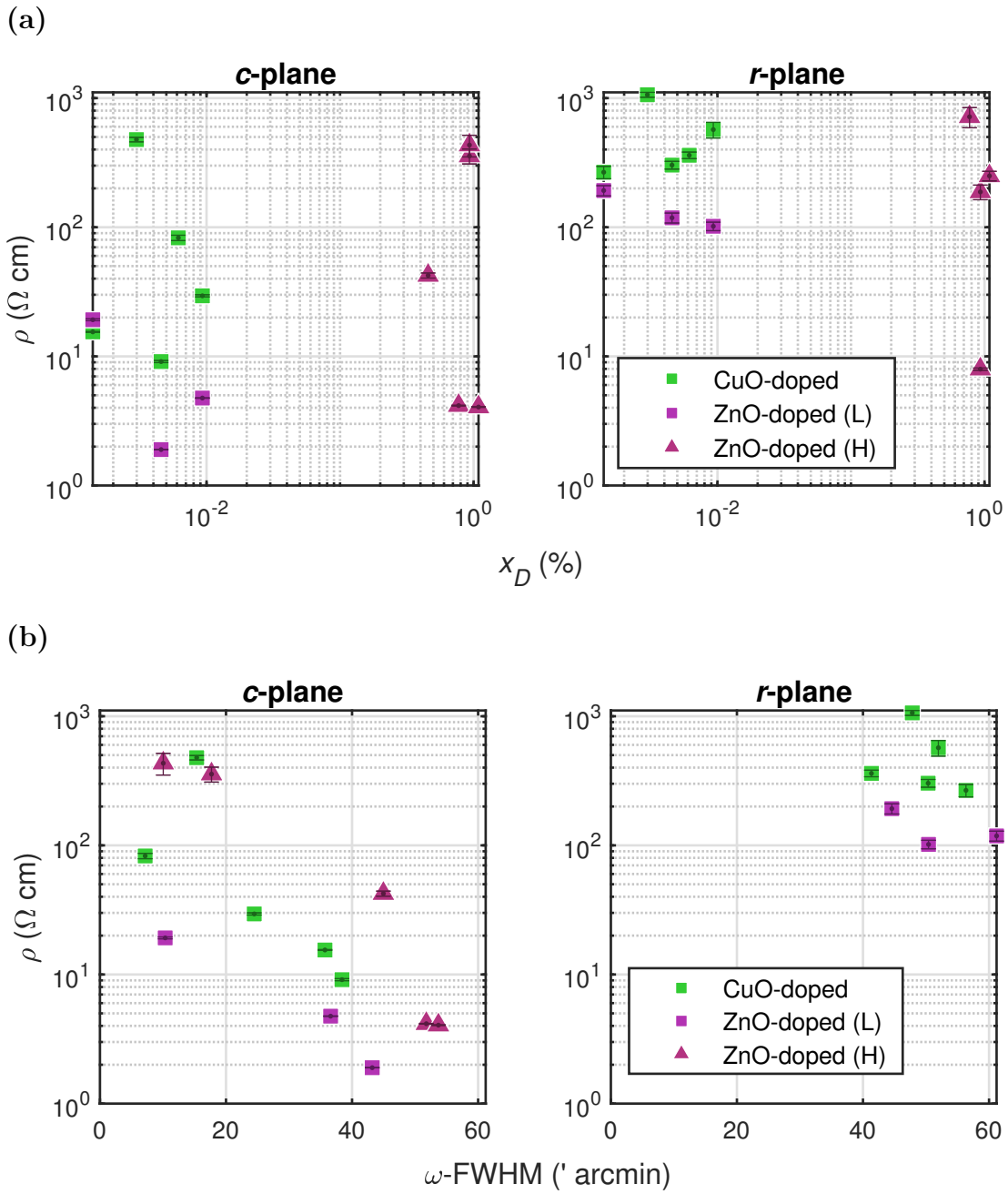

Figure 3.15: **(a)** Resistivity vs. predicted dopant concentration for c- and r-plane samples fabricated from all three radially segmented targets. **(b)** Resistivity vs. ω-FWHM of the aforementioned samples.

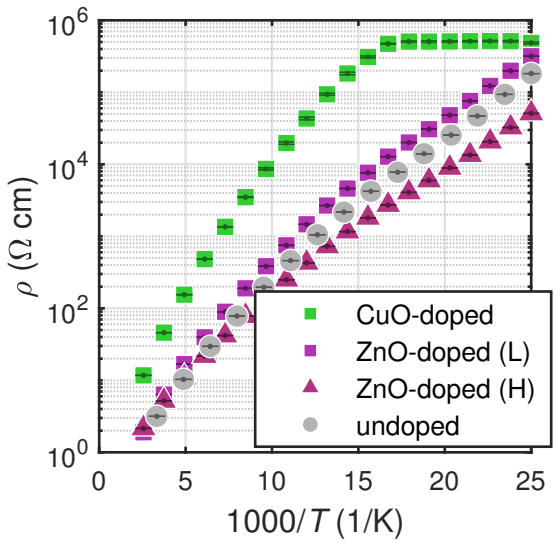

Figure 3.16: Temperature dependent resistivity measurements for *c*-plane samples fabricated from the different radially segmented targets, as well as a pure Cr_2O_3 target. The clipping of the sample from the CuO-doped target (green squares) is due to the limited resolution of the measurement device and the artifact nature of this saturation is confirmed by repeated measurements with different current applied during measurement (not shown).

Fig. 3.17a. For *m*- and *a*-plane, this behavior can indeed be observed. However, the slope of this relation differs depending on the target: the samples fabricated from the CuO-doped target showed less strain depending on growth rate than the samples fabricated from the ZnO-doped (high) target. This may be explained by the fact that the target degradation for the former (cf. Fig. 3.13a) was not so pronounced when compared to the latter (cf. Fig. 3.13c).

A reverse behavior is observed for *c*-plane samples: the strain is increasing with higher growth rates. But compared to *m*- and *a*-plane, there is no significant difference between the samples fabricated from different targets. This leads to the assumption that the plasma dynamics do not determine the o.o.p. strain for this orientation. It has to be noted that due to the constant pulse number, a change in growth rate corresponds to a change in thickness of the thin films. Therefore, it may be possible that the strain of the thin samples (low growth rate) is due to pseudomorphic growth on the correspoding Al_2O_3 substrate. Note that this leads not to the conclusion that the origin of the strain in *m*- and *a*-plane samples is also pseudomorphic growth: There, the thicker samples show more strain which is not expected because far away from the interface, dislocations should form to propagate relaxed growth. For *r*-plane samples, the overall strain is smaller and shows a less pronounced trend similar to *m*- and *a*-orientation. Because *r*-plane has both basal and prismatic character, both thickness and plsama dynamics effects may contribute to the observed strain.

The qualitative difference between *c*-plane and the other orientations can also be observed in Fig. 3.17b, where the ω-FWHM is shown depending on the o.o.p. strain. Compared to the previous results (cf. Fig. 3.7a), both factors characterizing crystal quality (strain and ω-FWHM) are not minimized simultaneously.

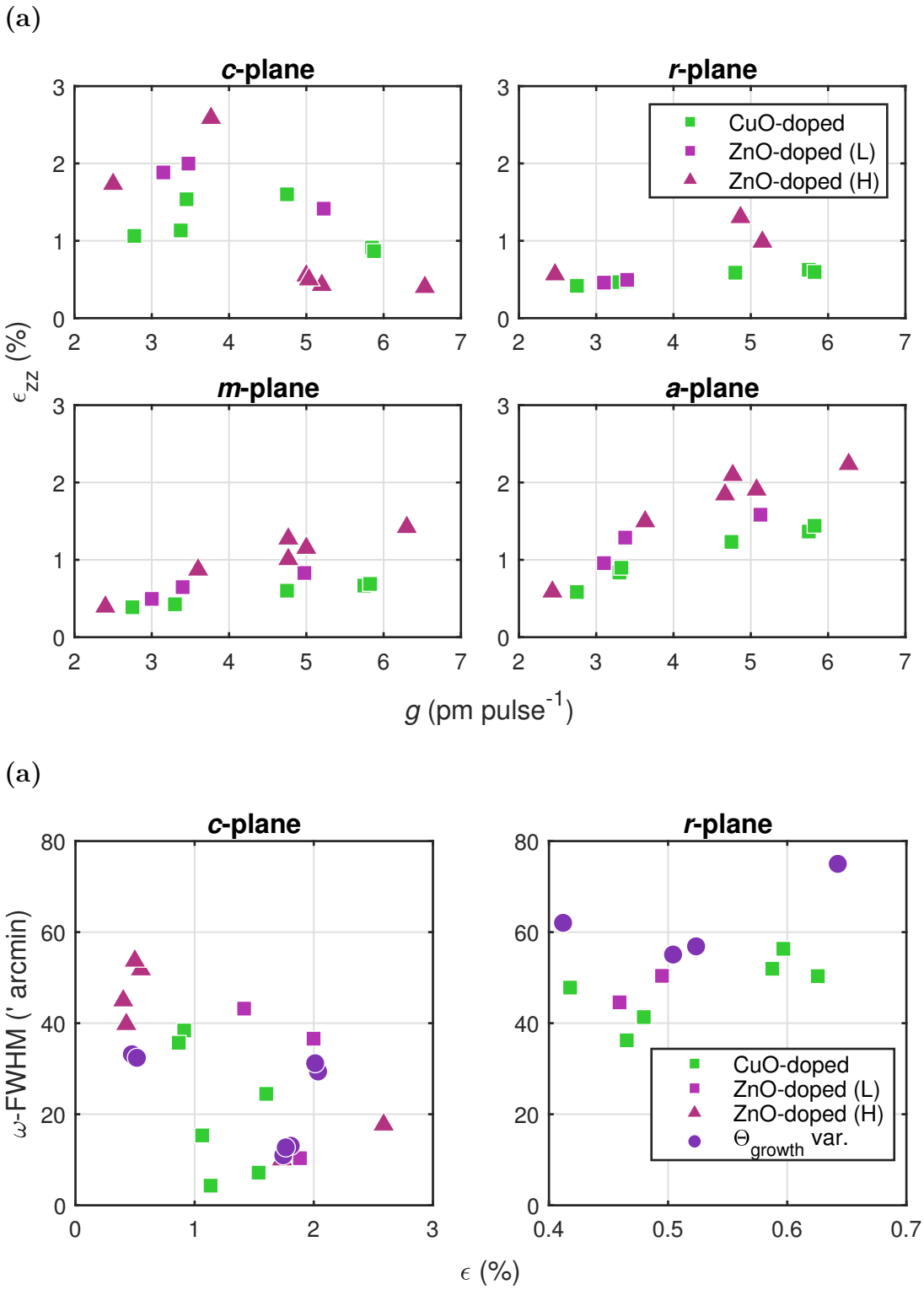

Figure 3.17: **(a)** Strain extracted from the peak positions in 2ϑ-ω-scans for samples fabricated from the three radially segmented targets. **(b)** Correlation between strain and ω-FWHM for *c*- and *r*-plane samples. The samples fabricated at differnt growth temperatures are also included.

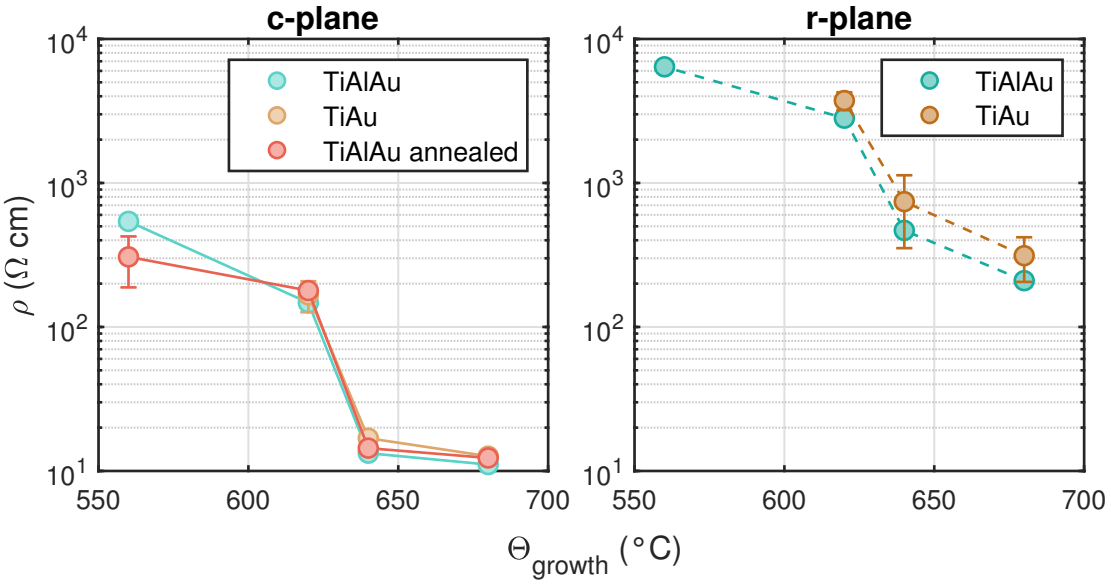

Figure 3.18: Resistivity measured at room temperature depending on growth temperature. Three different contact types were applied.

Ohmic Contact Optimization

For both *r*- and *c*-plane, a reduction in growth temperature results in higher crystallinity (not shown). Lower growth temperatures also yield higher resistivites, as shown in Fig. 3.18. This confirms the previously observed result, that the crystallinity reduces conductivity. It has to be noted that several effects influence the change in ω-FWHM: The first process was done at highest temperature, which was then gradually reduced. So the temperature reduction is convoluted with a process order effect. This is important, because for every sample, the same radial laser spot position $r_{\mathrm{PLD}} = 3\,\mathrm{mm}$ was used on the ZnO-doped (low) target, which led to increasing surface degradation (cf. Fig. 3.13b). This results, as shown before, in lower growth rates and higher crystallinities. This effect is supported by the fact that the window was cleaned before the first process only, which also adds to the subsequent reduction of laser fluence on the target surface. Therefore, the effect of temperature variation is covered by those growth rate effects, which makes it difficult to deconvolute the influence of growth temperature on conductivity. As can also be seen in Fig. 3.18, no significant change in resistivity was observed for both the variation between Ti-Al-Au and Ti-Au contacts, as well as between annealed and as-deposited contacts. For *r*-plane, the Ti-Al-Au contacts yielded slightly better conductivities.

3.2.3 Conclusion

The incorporation of CuO or ZnO had no effect on the conductivity of *c*- and *r*-plane oriented Cr_2O_3 thin films. None of the *m*- or *a*-plane oriented films became conductive. However, the conductivity depends strongly on the crystallinity, which indicates intrinsic defects as the origin of charge carriers. The crystallinity is mainly influenced by target degradation due to repeated ablation with the same laser spot position on the target. This results in lower growth rates and presumably less kinetic energy of

the plasma species which deposits on the substrate. Even though the doping attempt showed no effect, a discrete material library of Cr_2O_3 thin films with different strains was provided. A fundamental difference between *c*-plane and the other common orientations was observed, regarding the origin of the observed o.o.p. strain. Further measurements must be conducted to deconvolute the effects of (i) thickness, (ii) laser fluence on target and (iii) target degradation.

Bibliography

[1] L. Farrell et al. "Conducting mechanism in the epitaxial p-type transparent conducting oxide Cr_2O_3:Mg". In: *Physical Review B* 91.12 (2015), p. 125202. ISSN: 1098-0121, 1550-235X. DOI: 10.1103/PhysRevB.91.125202.

[2] Zhishan Mi et al. "The effects of strain and vacancy defects on the electronic structure of Cr_2O_3". In: *Computational Materials Science* 144 (2018), pp. 64–69. ISSN: 09270256. DOI: 10.1016/j.commatsci.2017.12.012.

[3] Chun-Shen Cheng, H. Gomi, and H. Sakata. "Electrical and Optical Properties of Cr_2O_3 Films Prepared by Chemical Vapour Deposition". In: *Physica Status Solidi (a)* 155.2 (1996), pp. 417–425. ISSN: 00318965, 1521396X. DOI: 10.1002/pssa.2211550215.

[4] M.F. Al-Kuhaili and S.M.A. Durrani. "Optical properties of chromium oxide thin films deposited by electron-beam evaporation". In: *Optical Materials* 29.6 (2007), pp. 709–713. ISSN: 09253467. DOI: 10.1016/j.optmat.2005.11.020.

[5] Max Kneiß et al. "Strain states and relaxation for α-$(Al_xGa_{1-x})_2O_3$ thin films on prismatic planes of α-Al_2O_3 in the full composition range: Fundamental difference of a- and m-epitaxial planes in the manifestation of shear strain and lattice tilt". In: *Journal of Materials Research* 36.23 (2021), pp. 4816–4831. ISSN: 0884-2914, 2044-5326. DOI: 10.1557/s43578-021-00375-3.